This is a repository copy of *Stearyl methacrylate-based polymers as crystal habit modifiers for triacylglycerols*.

White Rose Research Online URL for this paper:
http://eprints.whiterose.ac.uk/139043/

Version: Accepted Version

Article:
Jennings, J., Butler, M.F., McLeod, M. et al. (3 more authors) (2018) Stearyl methacrylate-based polymers as crystal habit modifiers for triacylglycerols. Crystal Growth and Design, 18 (11). pp. 7094-7105. ISSN 1528-7483

https://doi.org/10.1021/acs.cgd.8b01272

This document is the Accepted Manuscript version of a Published Work that appeared in final form in Crystal Growth and Design, copyright © American Chemical Society after peer review and technical editing by the publisher. To access the final edited and published work see https://doi.org/10.1021/acs.cgd.8b01272

Reuse
Items deposited in White Rose Research Online are protected by copyright, with all rights reserved unless indicated otherwise. They may be downloaded and/or printed for private study, or other acts as permitted by national copyright laws. The publisher or other rights holders may allow further reproduction and re-use of the full text version. This is indicated by the licence information on the White Rose Research Online record for the item.

Takedown
If you consider content in White Rose Research Online to be in breach of UK law, please notify us by emailing eprints@whiterose.ac.uk including the URL of the record and the reason for the withdrawal request.

eprints@whiterose.ac.uk
https://eprints.whiterose.ac.uk/

Stearyl Methacrylate-based Polymers as Crystal Habit Modifiers for Triacylglycerols

James Jennings*[1], Michael F. Butler[2], Madeleine McLeod[1], Evelin Csányi[1], Anthony J. Ryan[1], and Oleksandr O. Mykhaylyk*[1,3]

[1]Department of Chemistry, The University of Sheffield, Sheffield, S3 7HF, UK

[2]Unilever R&D, Colworth Lab, Bedford, MK44 1LQ, UK

[3]Soft Matter Analytical Laboratory, Department of Chemistry, The University of Sheffield, Sheffield, S3 7HF, UK

*Corresponding authors:

Oleksandr O. Mykhaylyk (o.mykhaylyk@sheffield.ac.uk) and James Jennings (james.jennings@sheffield.ac.uk)

Abstract

Triacylglycerides (TAGs) are ubiquitous and naturally-occurring fat molecules that can make materials with diverse textural, mechanical and optical properties. These properties are intimately linked to their complex hierarchical crystal structures, which can be controlled by additives that interfere with crystallization. A series of semi-crystalline bottlebrush-like copolymers has been developed to modify TAG crystallization and influence crystal habit. Synthesized by reversible addition-fragmentation chain transfer (RAFT) polymerization, these copolymer additives combine crystalline poly(stearyl methacrylate) with amorphous poly(oleyl methacrylate) in either block or statistical architecture. Upon cooling mixtures of these copolymers with solutions of tristearin (SSS) in triolein (OOO), the polymeric additives affected SSS crystallization at multiple length-scales. Microscopy analysis revealed control over SSS crystal morphology indicative of crystal aggregation, whilst small and wide angle x-ray diffraction (SAXD/WAXD) offered insight into the underlying mechanism of action. Analysing the physical broadening of lamellar peaks suggested that the fraction of amorphous poly(oleyl methacrylate) controls the thickness of primary nanoplatelets, and crystal structures derived from WAXD showed that the less stable α or β'-polymorphs of SSS are stabilized

by block or statistical copolymers, respectively. Exploiting these additives to simultaneously manipulate the packing of TAG molecules within lamellae, the size of primary crystallites, and the aggregation of crystallites could diversify fat material properties and supplement wide-ranging applications.

Introduction

The most abundant class of molecules that constitute fats are triacylglycerols (TAGs), which comprise three acyl chains attached to a central glycerol unit. Resulting from the many combinations of acyl chains that can be present in TAGs, the textural, mechanical and optical properties of fat mixtures are extremely diverse.[1] These properties are heavily dependent on the polymorph and morphology of solid fat crystals within the system, which can be tuned by affecting the fat composition and processing conditions used during fat crystallization[2]. TAG crystallization is a hierarchical process, in which individual TAGs organise into lamellar layers that stack on top of one another to make the primary crystallites.[3] These nanoplatelets can then further stack into structures commonly known as "TAGwoods",[4] which aggregate into 3-dimensional crystals and eventually crystal gels. Precisely controlling crystallization in fat mixtures at all of these stages is challenging, although strategies have been devised which employ additives to tune crystallization.[5-10] These additives include naturally occurring small molecules (sorbitan esters, sucrose esters, partial glycerols and phospolipids)[5, 6, 8-10] and polymers (polyglycerol fatty acids)[7], with molecular structures typically containing saturated fatty acid chains that interact with solid fats during crystallization.

Analysis of the complex TAG crystal structures necessitates the employment of several techniques in order to understand the materials at multiple lengthscales. The packing of acyl chains within lamellae is determined mainly from small-angle X-ray diffraction (SAXD) and wide-angle X-ray diffraction (WAXD), which provide information about the TAG crystal polymorphs. Polymorphs are distinguished by the number of acyl chains forming the crystal layer (measured by SAXD) and the arrangement of acyl chains within the lamellar layer including the degree of tilt relative to the lamellar normal (measured by WAXD). Meanwhile, macroscopic crystalline morphology that results from crystal aggregation can be imaged using optical microscopy techniques. Intermediate structures, such

as the primary crystallites composed of stacked lamellar layers, can be directly imaged using transmission electron microscopy. However, this technique is limited to sampling small populations of crystals, and sample preparation can be disruptive and perturb the true structure.[11] Employing non-destructive SAXD/WAXD enables sampling of larger and more representative volume of the sample, and can be performed in situ to follow crystallization kinetics. Peaks detected at small angles (i.e. SAXD) provide information about the thickness of individual lamellar layers in TAG crystals, but also allow characterization of TAG crystallite size. The shape and breadth of the crystalline lamellar peak contains information about the size of TAG crystallites and the presence of crystal lattice strain.

Fats applied in cosmetics (e.g. creams) and food (e.g. spreads), usually contain mixtures of saturated and unsaturated TAGs which at ambient conditions are usually crystalline and liquid, respectively.[12] As a result of low solubility and the ability to nucleate crystallization, saturated fats often provide material hardening properties, but have associated health issues. Therefore, it is desirable to replace saturated fats with healthier additives that influence crystallization and provide comparable properties. Effective additives to control TAG crystallization should comprise both constituents - saturated aliphatic chains that can interact with crystalline TAGs, and unsaturated chains that are compatible with amorphous TAGs remaining in the liquid state. In this paper a library of bottlebrush-like synthetic polymers with side chains comprised of fatty acid residues with modular structures are employed to control TAG crystallization in binary fat mixtures representing crystalline saturated and liquid unsaturated TAGs [tristearin (SSS) and triolein (OOO), respectively]. The crystallization process was followed in situ by conducting SAXD/WAXD analysis during cooling to determine the crystal polymorphs and estimate crystallite thickness. One convenient method to estimate crystallite thickness is to use the Scherrer analysis[11], which is calculated based on the breadth of the lamellar 001 reflection. The Williamson-Hall (WH) technique was employed in this study to characterize the size of primary fat crystallites, as it also employs higher order diffraction peaks to more accurately measure the size and strain present in TAG crystals, whilst optical microscopy allowed post-crystallization analysis of crystal aggregate structures. Results show that these side-chain crystalline polymers strongly influenced the crystallization of SSS in OOO, and studying the

process of SSS crystallization at multiple length-scales enabled a mechanism of crystal habit modification to be ascertained. These outcomes could significantly guide the design of materials based on fat crystals, allowing the selection of structures that lead to specific properties.

Experimental

Materials and methods. Glyceryl tristearate or tristearin (SSS, >96%, Sigma-Aldrich), glyceryl trioleate or triolein (OOO, >75%, Sigma-Aldrich), oleyl alcohol (>90%, Sigma-Aldrich), triethylamine (99%, Sigma-Aldrich), fluorescein O-methacrylate (97%, Sigma-Aldrich), toluene (99%, Sigma-Aldrich) and methanol (99%, Sigma-Aldrich) were used as received. Dicholoromethane (99%, Sigma-Aldrich) was dried using a Grubbs system. Stearyl methacrylate (≥97%, TCI) was dissolved in toluene and passed through a column of neutral alumina (Sigma-Aldrich) prior to use in order to remove inhibitors. Methacryloyl chloride (99%, Sigma-Aldrich) was distilled prior to use in synthesis. Azobisisobutyronitrile (AIBN, Fisher) was recrystallized twice from methanol. 2-Phenyl-2-propyl benzodithioate (CDB, 99%, Sigma-Aldrich) was used as received.

Synthesis of oleyl methacrylate. The procedure follows that of Hosta-Rigau et al.[13] Oleyl alcohol (15 g, 55.87 mmol) was dissolved in dry DCM (400 g) within a three-necked round bottom flask equipped with a stir bar. Triethylamine (21 ml, 150.6 mmol) was added under a flow of nitrogen and the flask submerged into an ice bath (ca. 0 °C). Methacryloyl chloride (12 ml, 122.8 mmol) was added dropwise under a flow of nitrogen, and the reaction mixture stirred overnight under a flow of nitrogen whilst slowly warming to room temperature overnight. Solvent was removed from the orange solution under vacuum, and the crude product dissolved in diethyl ether (200 ml). The organic solution was washed successively with 0.1M HCl (200 ml), saturated sodium bicarbonate (200 ml), water (200 ml), and then brine (200 ml). The organic layer was then dried over magnesium sulfate and solvent removed under vacuum. The resulting yellow oil was purified by column chromatography in a hexane/ethyl acetate (9/1) eluent, to give a clear oil (8.82 g, 47 % yield). ^{1}H NMR (conducted at 400 MHz in deuterated chloroform). Chemical shifts in ppm (multiplicity of peak, total number of protons,

identity of the proton) as follows: 0.87 (triplet, 3H, CH_2–C**H**$_3$), 1.18-1.41 (multiplet, 22H, side chain methylene), 1.66 (quintet, 2H, OCH_2–C**H**$_2$–), 1.88–2.08 (multiplet, 7H, O=C–C**H**$_3$ and −C**H**$_2$–CH=CH−C**H**$_2$−), 4.13 (triplet, 2H, OC**H**$_2$–), 5.28–5.44 (multiplet, 2H, −C**H**=C**H**–), 5.54 (singlet, 1H, methacrylate −C=C**H**), 6.09 (singlet, 1H, methacrylate −C=C**H**). Mass spectrometry (electron ionisation time-of-flight) gave mass/charge ratio of 336.3, compared to a theoretical value of 336.56 for $C_{22}H_{40}O_2$.

Synthesis of poly(stearyl methacrylate) homopolymer, S_{37}. Stearyl methacrylate (5.000 g, 14.76 mmol) was dissolved in toluene (5 ml) and passed through a column of neutral alumina, in order to remove the hydroquinone inhibitor, onto CDB (67.3 mg, 0.247 mmol) and AIBN (8.2 mg, 0.05 mol). The column was flushed with additional toluene (3.3 ml), and the reaction vessel sealed. The polymerization mixture was purged with nitrogen for 20 minutes, before being heated at 70 °C and stirred for 5 h. The polymer was purified by precipitation into methanol five times, and dried under vacuum. Degree of polymerization (DP) was measured by ^{1}H NMR in $CDCl_3$ to be 37. Number average molecular weight ($M_{n,GPC}$) and dispersity (Đ) were measured by gel permeation chromatography in THF ($M_{n,GPC}$ = 11.5 kg mol^{-1}, Đ = 1.15) (Table 1).

Synthesis of fluorescently-labelled poly(stearyl methacrylate) homopolymer, fS_{50}. Stearyl methacrylate (5.00 g, 0.0148 mol) was dissolved in 2 mL THF and passed through a column of inhibitor removers. Stearyl methacrylate was added to fluorescein-o-methacrylate (0.1976 g, 0.494 mmol), 2-pheyl-2-propyl benzodithioate (0.1349 g, 0.494 mmol) and azoisobutyronitirile (0.0162 g, 0.0988 mmol). The reactants were degassed with nitrogen for 20 minutes, then heated to 70 °C for 16 hours to polymerize. The degassing and heating cycle was performed in absence of light. After 16 hours, ^{1}H-NMR showed the reaction was complete. The product was precipitated from THF into methanol and was dried under vacuum.

Synthesis of poly(oleyl methacrylate) homopolymer, O_{67}. Oleyl methacrylate (0.511 g, 1.52 mmol) was dissolved in toluene (1 ml) and added to CDB (8.0 mg, 0.029 mmol) and AIBN (1.2 mg, 0.007 mol). The polymerization vessel was sealed and purged with nitrogen for 20 minutes, before being heated at 70 °C and stirred for 17 h. The polymer was purified by precipitation into methanol five

times, and dried under vacuum. DP (by ^{1}H NMR in $CDCl_3$) = 67, $M_{n,GPC}$ = 15.3 kg mol^{-1}, Đ = 1.15 (Table 1).

Synthesis of poly(stearyl methacrylate)-block-Poly(Oleyl methacrylate). A few compositions of this copolymer (**S_{37}-O_x**, where x denotes DP of 11, 26 or 138) have been synthesized (Table 1) using the same procedure. For brevity, only a synthetic protocol for **S_{37}-O_{138}** is presented. The synthesized poly(stearyl methacrylate), S_{37}, was weighed into a vial (0.1 g) along with oleyl methacrylate (0.537 g, 1.60 mmol) and AIBN (0.33 mg, 0.002 mmol). After dissolution in toluene (0.9 ml), the mixture was purged with nitrogen for 20 minutes. The polymerization mixture was then heated to 70 °C and stirred for 24 h, before being purified by precipitation into methanol five times. Polymers were characterized by ^{1}H NMR determine the degree of polymerization DP of the poly(oleyl methacrylate) block and mass fraction of stearyl methacrylate within the total copolymer (m_S) was measured by ^{1}H NMR in $CDCl_3$ to be 138 and 0.21, respectively. $M_{n,GPC}$ = 44.2 kg mol^{-1}, Đ = 1.10 (Table 1).

Synthesis of poly(stearyl methacrylate)-poly(oleyl methacrylate) statistical copolymer. A few compositions of this copolymer (**S_a**-stat-**O_b,** where a and b denote the number of **S** and **O** units in the copolymer, equal to 47, 26 or 23 and 17, 32 or 67, respectively) have been synthesized (Table 1) using the same procedure. For brevity, only a synthetic protocol for **S_{26}**-stat-**O_{32}** is presented. Stearyl methacrylate (0.2 g, 0.59 mmol) was dissolved in toluene (0.4 g) and passed through a column of neutral alumina, onto a mixture of oleyl methacrylate (0.2 g, 0.59 mmol), CDB (5.7 mg, 0.021 mmol) and AIBN (0.7 mg, 0.004 mol). The column was flushed with additional toluene (0.5 ml), and the reaction vessel sealed. The polymerization mixture was purged with nitrogen for 20 minutes, before being heated at 70 °C and stirred for 5 h. The polymer was purified by precipitation into methanol five times, and dried under vacuum. Total DP (by ^{1}H NMR in $CDCl_3$) = 58, m_S = 0.44, $M_{n,GPC}$ = 12.6 kg mol^{-1}, Đ = 1.15 (Table 1).

^{1}H NMR analysis. ^{1}H NMR spectra were recorded in $CDCl_3$ using a Bruker AV1-400 or AV1-250 MHz spectrometer, using 64 averaged scans per spectrum. End group analysis was performed to calculate the average number of monomers per chain. DP was calculated from the ratio of the peak

arising to the CH_2 adjacent to the methacrylate ester in the side chain (3.92 ppm, singlet, 2H) relative to the thiobenzoate signal (7.86 ppm, doublet, 2H).

Gel Permeation Chromatography (GPC) analysis. Number average molecular weight and dispersity were measured using a THF eluent in a GPC system equipped with two 5 μm Mixed C columns (30 cm in length) and a WellChrom K-2301 refractive index detector operating at wavelength 950 ± 30 nm. The mobile phase also included 2.0% v/v triethylamine and 0.05% w/v butylhydroxytoluene, and the flow rate was set to 1.0 mL min^{-1}. Calibration was achieved using 10 poly(methyl methacrylate) standards (M_p = 1280 to 330 000 g mol^{-1}).

Differential Scanning Calorimetry (DSC). Thermal analysis was conducted on a Perkin-Elmer Pyris 1 instrument. Homogeneous mixtures of polymer and SSS were prepared prior to loading in DSC pans by heating and stirring at 80 °C for 30 mins. Melting and crystallization temperatures of polymers and polymer/SSS mixtures were recorded during the second cycles of heating or cooling at a rate of 10 °C/min.

Optical Microscopy. Samples were placed on a glass slide under a cover slip for imaging on an Axio Scope A1 fluorescence microscope (Zeiss, Jena, Germany) equipped with AxioCam 1Cm1 monochrome and Axiocam 105 color cameras. Polarised light imaging (PLI) was conducted between two crossed polarisers using 10x, 20x and 40x magnification. For analysing fluorescently-labelled samples, the Zeiss filter set 38 (excitation 470/40 nm and emission 525/50 nm) was used. All images were collected and processed within the software Zen Lite 2014 supplied with the microscope.

Small and Wide Angle X-ray Diffraction. SAXD and WAXD patterns were collected simultaneously using Xuess 2.0 laboratory beamline (Xenocs, Sassenage, France) equipped with FOX 3D multilayered X-ray mirror and two sets of scatterless slits for beam collimation, two hybrid pixel area detectors (Pilatus 1M for SAXD and Pilatus 100k for WAXD, Dectris, Baden-Dattwil, Switzerland) and a liquid gallium MetalJet X-ray source (Excillum, Kista, Sweden), wavelength λ = 1.341 Å. SAXD patterns were recorded using a sample-to-detector distance of 1.235 m (calibrated using silver behenate standard). Glass (borosilicate) capillary tubes of 2.0 mm diametre (WJM-Glass

Muller GMBH, Berlin, Germany) were used as sample holders. Capillary-loaded samples were mounted in an HFSX350-CAP temperature-controlled hot-stage (Linkam Scientific, Tadworth, UK) for data collection. Two-dimensional SAXD and WAXD patterns were azimuthally integrated, normalized and background-subtracted using the Foxtrot software package (supplied with the laboratory beamline) to obtain 1D scattering profiles.

Controlled crystallization experiments. SSS (10 mg), OOO (190 mg) and polymer additives were weighed into a 2 mL vial and mixed by stirring at 70 °C for 30 minutes. While in the solution state, mixtures were transferred into glass capillaries via a syringe. Capillaries were then inserted into a capillary heating stage and placed on the laboratory beamline. After heating to 70 °C and holding for 5 minutes, the capillaries were cooled at a rate of 1 °C/min to 0 °C, during which time-resolved diffraction pattern frames were collected every minute. The frames were continued to be collected for at least 15 minutes while the sample was held isothermally at 0 °C. After the cooling experiment, an aliquot of the mixture was removed from the capillary by syringe and placed on a glass slide, before being imaged by polarised light microscopy.

Size-strain analysis. Due to the large aspect ratio of acyl chains within TAGs, these molecules form crystal structures in which one of the periods, corresponding to the layered packing motif, is significantly larger than the others. The period of the layer is usually proportional to the length of acyl chains forming the molecules and consequently provides information about type of chain packing. Depending on TAG composition two-chain (2L) or three-chain (3L) layer packing is usually found.[14, 15] Diffraction peaks originating from the layered structure localize in SAXD region and are well separated from the other diffraction peaks predominantly located in WAXD region and related to the transverse acyl chain order within the layers. The SAXD peaks of TAG layers belong to the same crystallographic direction <001> and commonly up to six peak orders are observed[15, 16]. These unique properties of TAG diffraction patterns can be conveniently used for peak broadening analysis to obtain detailed information about crystallite size and structural strain along the fat layer normal which is hardly accessible by other techniques. Since the shape of each peak is virtually unaffected by its neighbours, a number of previously developed approaches[17, 18] can be used for extracting size-strain

information. In particular, SAXD TAG pattern could be suitable for the most rigorous Warren-Averbach method based on Fourier transformation[19, 20], not mentioning methods using the peak integral breadth[21] and the peak profile shape[22, 23] analysis. The studied systems contain only a small concentration of crystalline component (SSS, 5 wt%) resulting in a relatively low diffraction signal-to-noise ratio which significantly complicates an application of the Fourier methods. In this respect a technique based on the peak integral breadth involving a more statistically robust peak fitting procedure has been chosen for the size-strain analysis.

In order to perform the analysis a physical broadening of the peaks has to be obtained. The integral breadth of the diffraction peaks originating from the layered packing of TAGs can be calculated either from the peak profile function or from Fourier transform of the profile[24]:

$$\beta_{\mathrm{f}} = \frac{\int \mathrm{I_f}(2\theta)\mathrm{d}\,2\theta}{\mathrm{I_f}(2\theta_{\max})} = \frac{\mathrm{F_f}(0)}{\int \mathrm{F_f}(\mathrm{t})\mathrm{dt}} \qquad (1),$$

where $I_f(2\theta)$ is the peak profile function associated with the sample microstructure, $I_f(2\theta_{\max})$ is the peak maximum intensity, $F_f(t)$ is Fourier transform of the profile function. A convolution of the $I_f(2\theta)$ and $I_g(2\theta)$, describing instrumental effect on the peak broadening is registered experimentally:

$$I_h(2\theta) = \int I_f(u) I_g(2\theta - u)du \qquad (2),$$

which complicates calculation of the integral breadth β_f from the peak profile function using eq 1. The task can be simplified if eq 2 is rewritten via Fourier transforms of $I_h(2\theta)$, $I_f(2\theta)$ and $I_g(2\theta)$:

$$F_h(t) = F_f(t)F_g(t) \qquad (3),$$

which enables the Fourier transform of the physical profile function to be easily extracted as

$$F_f(t) = \frac{F_h(t)}{F_g(t)} \qquad (4)$$

and used for integral breadth calculations following the second part of eq 1. Practically, $F_h(t)$ and $F_g(t)$ can be calculated from the results of peak fitting using an analytical function with a known Fourier transform. In addition to the $I_h(2\theta)$ recorded from studied samples a standard sample has to be measured in order to obtain $I_g(2\theta)$. In this work pseudo-Voigt function, proven to be the most suitable to describe diffraction peaks[25], has been used to fit 00l reflections originating from TAG layered structure:

$$I(2\theta) = I(2\theta_{\max})[\eta L(2\theta) + (1-\eta)G(2\theta)] \quad (5),$$

where $L(2\theta) = \left[1 + \frac{(2\theta - 2\theta_{\max})^2}{\omega^2}\right]^{-1}$ is Lorentzian component and $G(2\theta) = \exp\left[-\ln 2 \frac{(2\theta - 2\theta_{\max})^2}{\omega^2}\right]$ is Gaussian component. A spectral composition of the Gallium characteristic radiation $K\alpha$ doublet used for the measurements was counted during the fitting. $2\theta_{\max}$ in eq 5 is assigned to the $K\alpha_1$ peak maximum position, 2ω is the full width at half maximum (FWHM) of the $K\alpha_1$ or $K\alpha_2$ diffraction profile which is assumed to be equal for both $\mathrm{L}(2\theta)$ and $\mathrm{G}(2\theta)$ components, η is the Lorentzan content and $I(2\theta_{\max})$ is the intensity at the $K\alpha_1$ peak maximum. The Fourier transform of pseudo-Voight function represented by eq 5 is expressed as

$$F(t) = I(2\theta_{\max})\omega\left[\eta\pi\exp(-2\pi\omega t) + (1-\eta)\left(\frac{\pi}{\ln 2}\right)^{1/2}\exp\left(-\pi\omega^2\frac{\pi}{\ln 2}t^2\right)\right] \quad (6).$$

It has been found that all fitted peaks of the studied samples have $\eta > 0.8$ indicating strong Lorentzian character of the peak profiles. Following this observation it has been assumed that a linear version of Williamson-Hall method derived for Lorentzian diffraction peaks[21, 26] would be a good approximation to perform size-strain analysis:

$$\beta_f^* = \beta^S + \beta^D = \frac{1}{D_{WH}} + (2\pi)^{1/2} e_{WH} d^* \quad (7),$$

where the measured physical broadening of a peak β_f and the period of an associated crystallographic plane d is converted into reciprocal space units ($s = 2\sin\theta/\lambda$) $\beta_f^* = \frac{\beta_f \cos\theta_{max}}{\lambda}$ and $d^* = 1/d$, respectively. β^S is d^*-independent size broadening component represented by Scherrer equation and β^D is d^*-dependent strain broadening component represented by an expression for the apparent strain derived from Bragg's law differentiation[26, 27]. Keeping in mind a certain degree of arbitrariness D_{WH} and e_{WH} correspond to crystallite size and strain along <001>, respectively. A straight line fitted to Williamson-Hall plot of physical broadening values of the peaks corresponding to the same crystallographic direction (or plane) will give $1/D_{WH}$ and $(2\pi)^{1/2} e_{WH}$ as the line intercept at $s = 0$ and the line slope in a respect to s-axis, respectively.

Before peak broadening analysis background scattering of liquid OOO component was subtracted from the entire SAXD patterns recorded during SSS crystallization. For this X-ray scattering of a pure OOO was recorded at the equivalent temperatures. This operation helped to improve peak-to-noise ratio of 001 and 003 lamellar peaks of SSS polymorphs formed by 2L TAG packing. In addition, Lorenz corrections of the obtained patterns were applied in order to remove an effect of the most pronounced θ-dependent term caused by the instrumental geometry[28]. Thus, the SAXD patterns were renormalized and plotted as 2θ versus $I(2\theta)\sin^2\theta\cos\theta$ before the 001 and 003 peak fitting using WinPLOTR® software[29]. The $I_g(2\theta)$ instrumental broadening function, eq 2, was determined by carrying out measurements of high purity SSS crystallized in the β-phase from solution (≥99%, Fluka).

Results and Discussion

Synthesis and characterization of additives for fat crystallization

Useful TAG-based materials commonly comprise mixtures of saturated molecules that make up the fat crystals (e.g. tristearin and tripalmitin), unsaturated molecules that comprise the oil matrix (e.g. triolein and trilineolein), in addition to TAGs with a mixture of saturated and unsaturated acyl

chains. In this study, a simplified binary mixture of saturated tristearin (SSS) and unsaturated triolein (OOO) was employed to allow better understanding of the mechanisms by which polymeric additives control TAG crystallization. A library of bottlebrush-like polymers were synthesized based on monomers with saturated (stearyl methacrylate, **S**) and unsaturated side chains (oleyl methacrylate, **O**) that matched the TAG components. Two distinct architectures were designed, in which the monomers were arranged in blocks or distributed throughout the chain (Figure 1), to study the effect of monomer sequence and overall polymer crystallinity within additives. Using a controlled/living radical polymerization technique (RAFT) allowed the synthesis of polymers with well-defined molecular weights and molecular weight distributions to be performed.[30] Furthermore, sequential addition of monomers during a RAFT polymerization enables the synthesis of well-defined block copolymers to be carried out.[31]

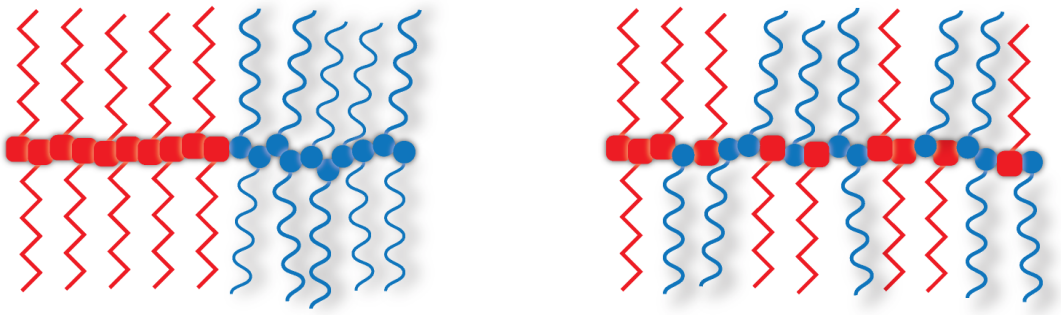

Figure 1. Schematic of polymeric additives employed to control fat crystallization in this study: saturated (red) and unsaturated (blue) copolymer components are either arranged in blocks (left) or in a statistical distribution throughout the polymer chain (right).

Homopolymers of stearyl methacrylate ($\mathbf{S_{37}}$) and oleyl methacrylate ($\mathbf{O_{67}}$) were first synthesized using the dithiobenzoate RAFT agent CDB. A series of block copolymers ($\mathbf{S_{37}}$-$\mathbf{O_x}$, where x is the number average degree of polymerization of oleyl methacrylate) were then synthesized by chain extension of $\mathbf{S_{37}}$ macro-RAFT agent with different quantities of oleyl methacrylate (Figure 2A). From this series of block copolymers, the influence of amorphous block fraction on SSS crystallization could be determined. It was initially hypothesised that the crystalline block would interact with the SSS crystals, while the amorphous block may act as a steric stabilizer and reduce aggregation of fat crystals. Statistical copolymers ($\mathbf{S_a}$-stat-$\mathbf{O_b}$) were synthesized by mixing different

proportions of the two monomers at the beginning of the reaction, which leads to a distribution of monomers throughout the chain determined by the monomer reactivity ratios.

The monodisperse appearance of GPC traces and low dispersity in all samples (Table 1 and Figures 2B-2D) confirms a well-controlled RAFT polymerization of **S** and **O**, and the successful chain extension into block copolymer was evidenced by the peak shift towards lower retention time (i.e. higher molecular weight) of $\mathbf{S_{37}}$-$\mathbf{O_x}$ relative to $\mathbf{S_{37}}$ precursor (Figure 2C). DSC analyses performed within the temperature range of controlled crystallization experiments (i.e. from 0 °C to 70 °C) confirmed that $\mathbf{S_{37}}$, all block copolymers, and $\mathbf{S}_{47}$-stat-$\mathbf{O}_{17}$, were semi-crystalline in nature. However, the statistical copolymers $\mathbf{S}_{26}$-stat-$\mathbf{O}_{32}$ and $\mathbf{S}_{23}$-stat-$\mathbf{O}_{67}$ did not display melting or crystallization transitions, and these polymers remain amorphous under these crystallization conditions.

Table 1: Characteristics of the polymers used as additives to control the crystallization of SSS: M_n is number average molecular weight, Đ is dispersity, m_S is the mass fraction of stearyl methacrylate within the total copolymer, T_m is the polymer melting point and T_c is the polymer crystallization temperature.

Polymer	M_n /kg mol^{-1}	Đ	m_S	T_m/°C[&]	T_c/°C[&]
$\mathbf{S_{37}}$	12.0	1.15	1	33.1	27.3
$\mathbf{fS_{50}}$	14.0	1.13	1	33.6	25.4
$\mathbf{S_{37}}$-$\mathbf{O_{11}}$	14.1	1.13	0.76	29.5	22.7
$\mathbf{S_{37}}$-$\mathbf{O_{26}}$	16.8	1.14	0.59	28.8	21.6
$\mathbf{S_{37}}$-$\mathbf{O_{138}}$	44.2	1.10	0.21	28.6	19.1
$\mathbf{S_{47}}$-stat-$\mathbf{O_{17}}$	16.3	1.16	0.77	28.0	16.7
$\mathbf{S_{26}}$-stat-$\mathbf{O_{32}}$	12.6	1.15	0.44	< 0	< 0
$\mathbf{S_{23}}$-stat-$\mathbf{O_{67}}$	18.7	1.20	0.29	< 0	< 0
$\mathbf{O_{67}}$	15.3	1.15	0	< 0	< 0

[&]Taken from the onset of melting or crystallization, measured by DSC during a heating cycle between 0 °C and 70 °C at a heating or cooling rate of 10 °C/min

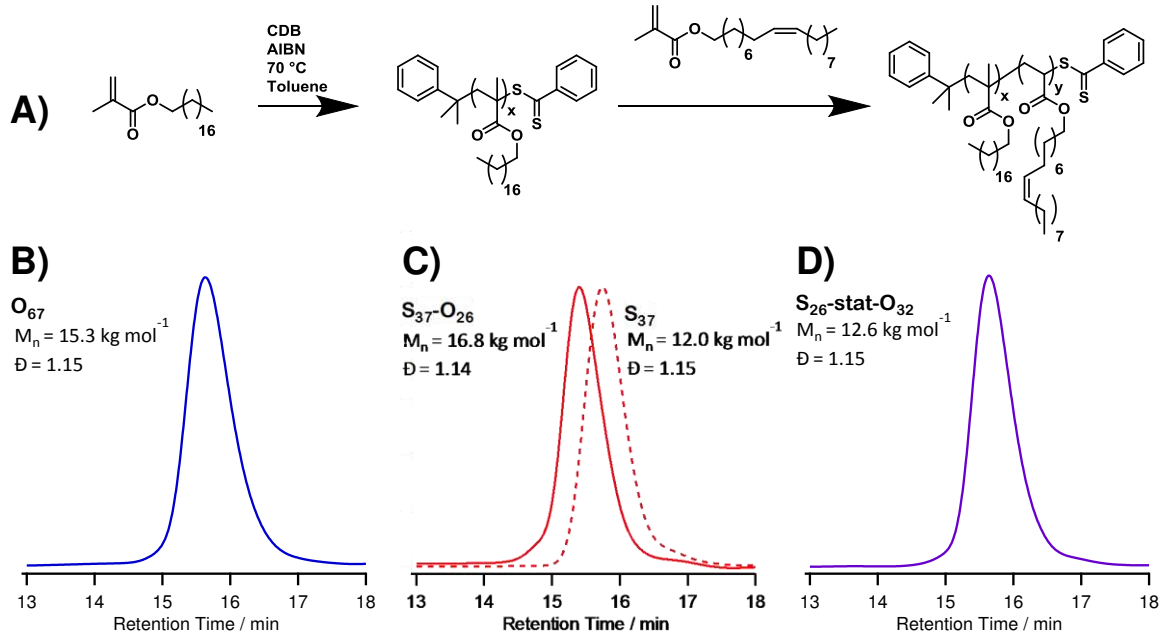

Figure 2. A) Reaction scheme for the synthesis of stearyl-oleyl methacrylate block copolymers ($\mathbf{S_x}$-$\mathbf{O_y}$) and representative GPC traces of B) poly(oleyl methacrylate), $\mathbf{O_{67}}$ C) poly(stearyl methacrylate) $\mathbf{S_{37}}$ (dashed line) and stearyl-oleyl methacrylate block copolymer $\mathbf{S_{37}}$-$\mathbf{O_{26}}$ (solid line) and D) stearyl-oleyl methacrylate statistical copolymer, $\mathbf{S_{26}}$-stat-$\mathbf{O_{32}}$.

Crystal morphology

Initial observations into the effect of polymer additives on TAG crystallization were made using the model system of 5 wt% SSS in OOO solution using both bright field and polarised light microscopy. A low concentration of SSS was chosen to minimise aggregation of fat crystals, whilst providing a sufficient concentration of crystals to allow characterization by SAXD and WAXD analysis. Each mixture of SSS and OOO was combined with a specific amount of polymer additive, such that the molar ratio of stearyl methacrylate to tristearin was constant (1:2). Images were captured immediately after cooling at a rate of 1 °C/min from 70 °C to 0 °C in borosilicate capillary tubes that were used as sample holders for SAXD/WAXD measurements. The model system sample formed large and polydisperse aggregates of 10 to 50 µm in diameter (Figure 3A). These aggregates were composed of randomly oriented crystals of much smaller sizes, and such dendritic structures are commonly encountered in TAG crystallization as a result of aggregation.[1]

The introduction of polymeric additives significantly altered the morphology of SSS crystals, and crystal morphology was dependant on the fraction of amorphous **O** component in the polymer additive (Figure 3B-F). In the presence of stearyl methacrylate homopolymer (**S_{37}**), crystals were mostly short needle-like structures <10 µm in length (Figure 3B). SSS crystals grown in the presence of **S_{37}-O_{26}** were longer needles and more aggregated (Figure 3D). When the length of the O block was increased to 138 monomer units, uniform spherulitic particles were formed with an average diameter of <10 µm (Figure 3E). The three dimensional nature of these crystals was evident in the appearance of the maltese cross texture when viewed between crossed polarisers, which suggested that the crystals were oriented parallel or perpendicular to the plane of polarised light. Crystallization in the presence of oleyl methacrylate homopolymer (**O_{67}**) resulted in randomly aggregated crystals (Figure 3C) resembling crystals formed in the absence of additives. Finally, SSS crystals formed in the presence of **S_{26}**-stat-**O_{32}** were a mixture of spherulites and needle-like objects (Figure 3F).

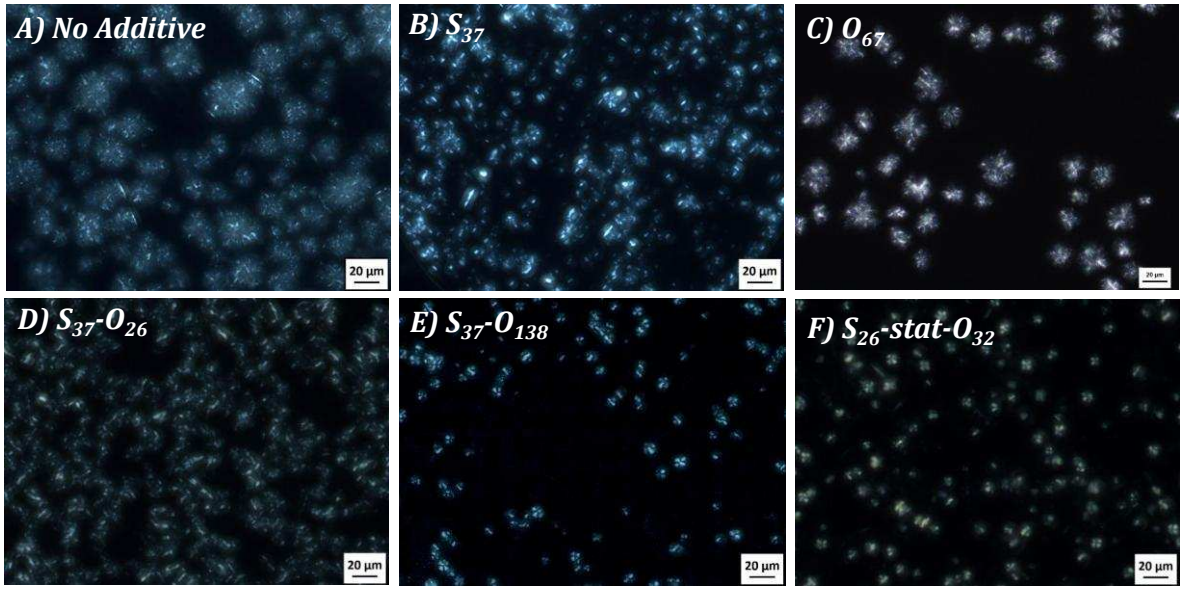

Figure 3. Polarised light microscopy images of SSS crystals prepared after cooling 5 wt% SSS in OOO solution blended with different polymer additives (indicated at the top left corner of the images) from 70 °C to 0 °C at a rate of 1 °C/min. A scale bar of 20 µm is shown at the bottom right corner of each image.

To obtain visual proof of the location of polymers on SSS crystals, a fluorescently-labelled analogue of poly(stearyl methacrylate) (**fS_{50}**) was synthesized, added to a solution of SSS (5 wt% in OOO) and crystallized by cooling at 1 °C/min. Images taken on a fluorescent microscope revealed

that all crystals were uniformly fluorescent in appearance, signifying that there was an intimate co-crystallization between the polymer additive and SSS (Figure 4). Since the primary crystallites involved in TAG crystallization (i.e. nanoplatelets) are typified by dimensions < 100nm,[2] optical microscopy allows only the higher hierarchical structures that arise from aggregation of smaller crystallites to be observed. In general, the presence of side-chain crystalline (**S**-containing) polymers influenced the aggregation of SSS crystallites, and inhibited the formation of large dendritic crystals and gels that are characteristic of TAG mixtures without additives. It was also clear that the fraction of **O** component within the copolymer systems was a key feature determining crystal morphology. To gain further insight into the mechanism of crystal habit modification at a molecular level, in-depth analyses were performed using SAXD and WAXD.

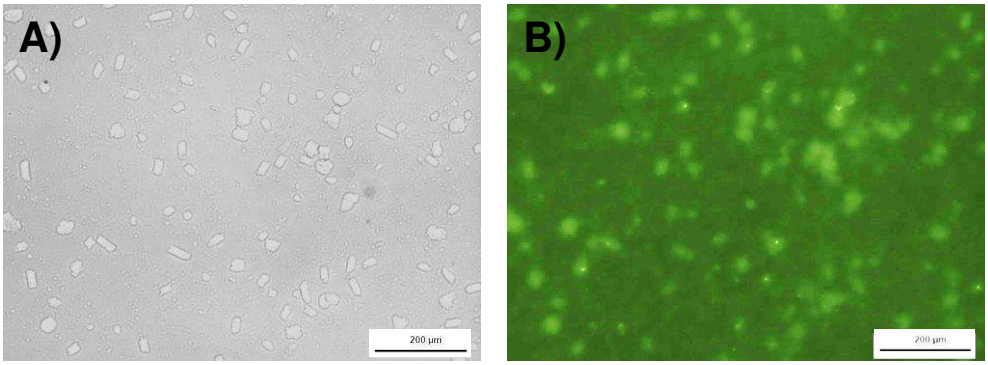

Figure 4. Bright field (A) and fluorescent image (B) at 20× magnification, showing SSS crystals (5 wt% in OOO) prepared after cooling from 70 °C to 0 °C at a rate of 1 °C/min in the presence of **fS$_{50}$**. The images demonstrate the localisation of polymer within the SSS crystals.

Kinetics of crystallization

The crystallization process was followed in situ by simultaneous SAXD/WAXD performed while cooling mixtures of SSS, OOO and polymer additives within glass capillaries. SAXD data provided information on the onset of SSS crystallization from the point at which the first Bragg peaks resulting from lamellar packing of TAGs appeared, while WAXD data allowed determination of the crystal polymorphs. Upon cooling a 5 wt% SSS solution in OOO, the onset of crystallization occurred at ~ 23 °C (Figure 5A), as determined by the appearance of an initial lamella 001 peak at s = 0.020 Å^{-1}. At 22 °C, a higher order 003 peak becomes visible at 0.061 Å^{-1}. These peak positions indicate a layer spacing of 49.6 Å, which is consistent with the α-phase of SSS.[32] Upon further cooling to 20 °C,

a shoulder on the 001_α reflection was apparent. At 17 °C the 001_α and 003_α peaks disappeared and were replaced by a Bragg peak with a maximum at s = 0.022 $Å^{-1}$ and a higher order peak at 0.067 $Å^{-1}$. The lamellar spacings calculated based on the second series of peaks corresponded to 45.1 Å, consistent with the β-phase of SSS.[33] Evidently, SSS underwent a spontaneous transition from α-phase to β-phase during the cooling cycle. It has to be noted that 002 peaks for α and β phases were either extinct or had vanishingly small intensities. Similar behaviour was observed in the presence of $\mathbf{O_{67}}$; the onset of SSS crystallization was at 22 °C, and 001_α and 003_α initially observed at the point of nucleation disappeared and were replaced by 001_β and 003_β peaks, suggesting that the final sample consisted of β-phase SSS crystals. The similarity in crystallization observed by SAXD (Figures 5A and 5B) is consistent with the similarity in crystal morphologies observed by microscopy (Figures 3A and 3C).

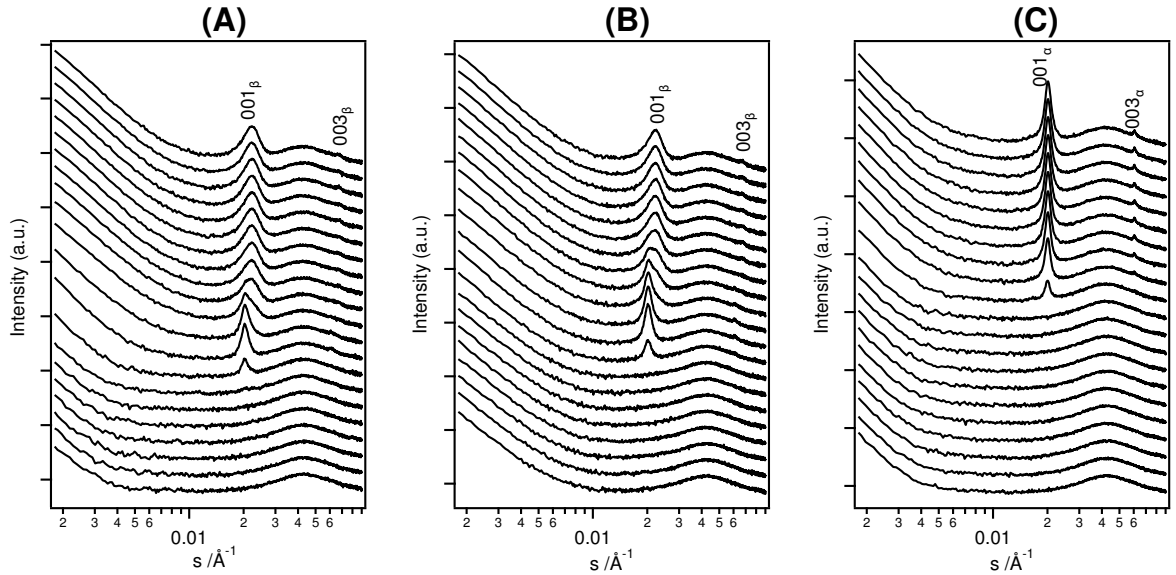

Figure 5. Time-resolved SAXD data for crystallization of SSS from solution (5 wt% in OOO) while cooling from 30 °C (bottom pattern) to 10 °C (top pattern) at a rate of 1°C/min: A) without polymer additives and in the presence of B) $\mathbf{O_{67}}$, and C) $\mathbf{S_{37}}$. SAXD peaks of β- and α-phase of SSS are indicated by Miller indices.

In the presence of the $\mathbf{S_{37}}$, the onset of crystallization was postponed to 19 °C (Figure 5C), and no polymorphic transition took place: SSS crystallized in the α form, and remained in that polymorph as the temperature was decreased to 0 °C. Comparison of SAXD data collected while cooling SSS in the presence of stearyl-oleyl methacrylate block copolymers and statistical copolymers

provided insight into the effect of polymer architecture on the fat crystallization. With the block copolymer additives, the onset of SSS crystallization was lowered to between 14 °C and 18 °C, and all block copolymers stabilized the α-phase, preventing transition into β-phase (Figure 6A-C). Meanwhile, in the presence of statistical copolymer additives (**S$_a$**-stat-**O$_b$**), very different behaviour was observed depending on the ratio of monomers (Figure 7). When the copolymer comprised a majority of **S** (**S$_{47}$**-stat-**O$_{17}$**), behaviour was similar to the block copolymers: the onset of crystallization was delayed until 14 °C, and the α-phase persisted throughout the cooling cycle (Figure 7A). However, in the presence of **S$_{26}$**-stat-**O$_{32}$**, SSS underwent a partial polymorphic transition (Figure 7B). A primary peak at s = 0.020 Å^{-1} was observed upon nucleation at 22 °C (001_α), but below 18 °C a shoulder appeared at the high s side and both peaks persisted for the duration of the cooling experiment. The same behaviour was observed in the mixture containing **S$_{23}$**-stat-**O$_{67}$** (Figure 7C), and the second peak position could be more easily resolved (s = 0.022 Å^{-1}). In the presence of **S$_{26}$**-stat-**O$_{32}$** and **S$_{23}$**-stat-**O$_{67}$**, it appeared that the coexistence of α and β phases persisted for the duration of the cooling cycle.

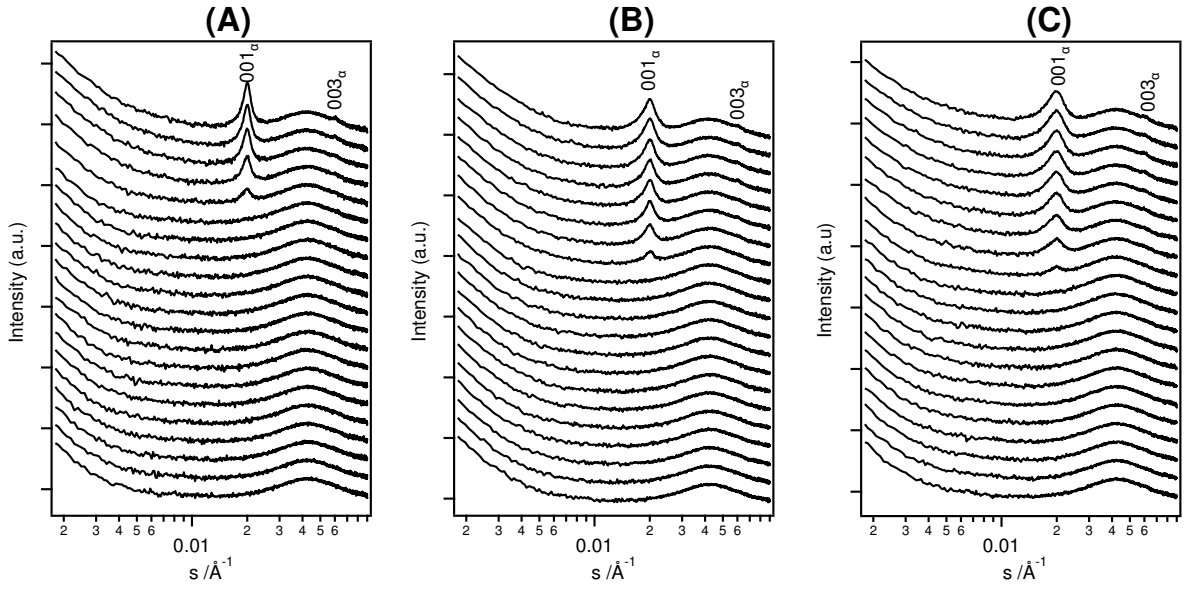

Figure 6. Time-resolved SAXD data for crystallization of SSS from solution (5 wt% in OOO) while cooling from 30 °C (bottom pattern) to 10 °C (top pattern) at a rate of 1°C/min in the presence of A) **S$_{37}$-O$_{26}$**, B) **S$_{37}$-O$_{26}$**, and C) **S$_{37}$-O$_{138}$**. SAXD peaks of α-phase of SSS are indicated by Miller indices.

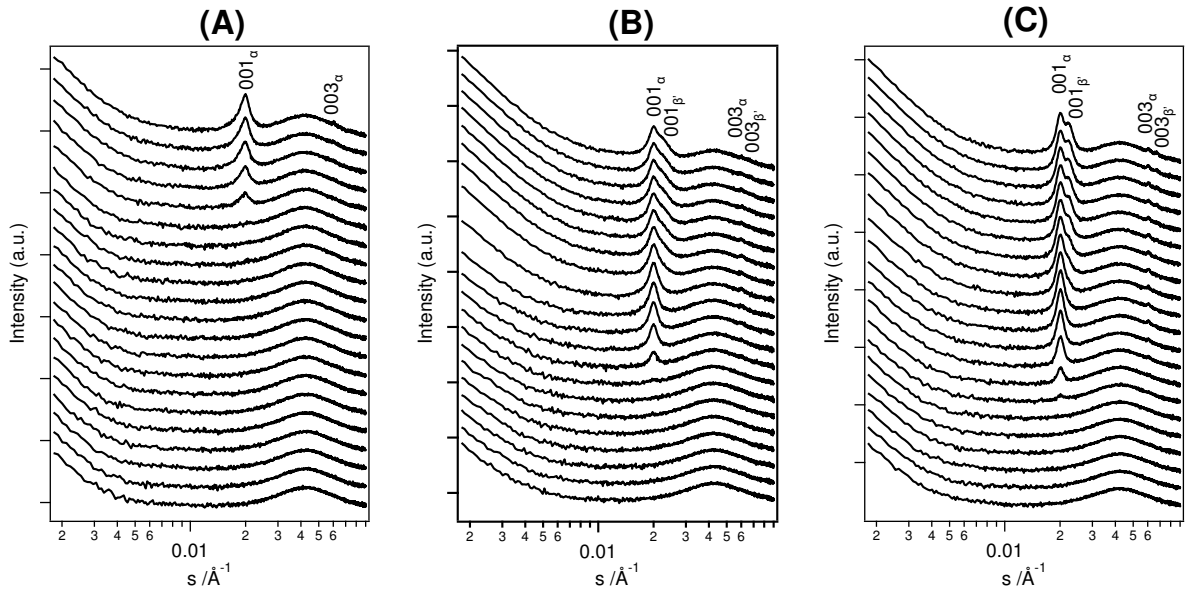

Figure 7. Time-resolved SAXD data for crystallization of SSS from solution (5 wt% in OOO) while cooling from 30 °C (bottom pattern) to 10 °C (top pattern) at a rate of 1°C/min in the presence of A) **S$_{47}$**-stat-**O$_{17}$** B) **S$_{26}$**-stat-**O$_{32}$**, and C) **S$_{23}$**-stat-**O$_{67}$**. SAXD peaks of α-, β'- and β-phase of SSS are indicated by Miller indices.

S$_{37}$, **S$_{37}$-O$_x$** block copolymers, and **S$_{47}$**-stat-**O$_{17}$** additives all lowered the temperature at which SSS crystallized during the controlled cooling experiments, which confirms that the presence of a stearyl side chain within the additive is a key feature enabling control over SSS crystallization. Indeed, additives employed for controlling fat crystallization in prior studies often contain alkyl groups with similar chain lengths as the TAGs being crystallized.[5-9] Additives in fat crystallization commonly act by promoting crystallization, but the observed depression of crystallization temperature in this study suggests that these polymeric additives do not act as nucleation sites for SSS. The mechanism of crystallization retardation could have a kinetic or thermodynamic origin: either the rate of nucleation was decreased, or the supersaturation concentration of SSS in the presence of polymer is reduced. To distinguish these two possibilities, isothermal crystallization was attempted at 30 °C by cooling a solution of SSS (5 wt% in OOO) alone, and in the presence of **S$_{37}$** polymer, from solution (70 °C) at a rate of 1 °C/min. In the mixture without additives, SAXD demonstrated formation of SSS lamellar peaks after < 10 min at 30 °C, whilst the mixture containing **S$_{37}$** did not crystallize over a period of 18 hours. Furthermore, upon heating samples from 0 °C at 1 °C/min, lamellar peaks were

found to disappear at a lower temperature in the presence of $\mathbf{S_{37}}$ (45 °C vs. 47 °C). These observations strongly suggest that the polymer altered the supersaturation concentration of SSS in OOO. In other words, the lower crystallization and melting temperatures in the presence of additives with an **S** block correspond to an increase in solubility of SSS in OOO. This may be the result of strong van der Waals' interactions between stearyl side chains of polymers and SSS alkyl chains in solution, which inhibit the formation of SSS nuclei upon cooling. The fact that SSS crystallization temperature remains almost unchanged in the presence of either $\mathbf{O_{67}}$, $\mathbf{S_{26}}$-stat-$\mathbf{O_{32}}$ and $\mathbf{S_{23}}$-stat-$\mathbf{O_{67}}$ suggests that a continuous block of monomers with stearyl side chains is a key structural motif to interfere with SSS crystallization.

Polymorph analysis.

The WAXD region containing peaks originating from the transverse acyl chain order within the layers is considered to be a fingerprint of TAG polymorphs[14, 33] which allows more accurate assignment of phase composition than lamella peak positions and associated d-spacings measured from SAXD. Due to the low concentration of crystalline material within the fat mixtures (ca. 5 wt%), analysis of the WAXD peaks arising from SSS crystals are largely hindered by the broad peak originating from OOO molecules in the liquid state. To remedy this, a background scattering of OOO measured at the same temperature was subtracted from WAXD data of SSS in OOO blends (see an example of the subtraction procedure in the Supporting Information, Figure S1). Subtracted WAXD data collected after cooling the mixture of SSS and OOO to 0 °C revealed multiple peaks, with at least 3 peaks resolved at s = 0.216, 0.255 and 0.268 $Å^{-1}$ (Figure 8A). These peak positions are consistent with three of the strongest reflections arising from a triclinic unit cell of the β-phase (101, $20\bar{1}$, $3\bar{1}0$, respectively[34]),[33] the most thermodynamically stable in triacylglycerols. Within this polymorph, TAGs adopt a chair conformation, and alkyl chains are arranged with a degree of tilt relative to the lamellar crystal normal. The same peak signature was observed for SSS crystallized in the presence of $\mathbf{O_{67}}$ (Figure S2A).

WAXD data collected after cooling the mixture of SSS and OOO to 0 °C in the presence of **S_{37}**, **S_{37}-O_{11}**, **S_{37}-O_{26}** or **S_{37}-O_{138}** all showed only one WAXD peak at ca. 0.240 $Å^{-1}$ (Figures 8B and S2B-S2D). This is consistent with the α-phase of SSS crystals, and corresponds to the average chain-to-chain distance within hexagonally-packed alkyl chains arranged normal to the lamellar interface.[33] This single 100_α peak was also observed initially upon nucleation, and persisted upon cooling to 0 °C. Meanwhile, SSS crystallized in the presence of **S_{26}**-stat-**O_{32}** and **S_{23}**-stat-**O_{67}** additives revealed two distinct peaks in the subtracted WAXD data at s = 0.238 $Å^{-1}$ and 0.263 $Å^{-1}$ (Figure 8C). Although the former peak could be assigned as α-phase, the latter peak is ambiguous. The observed pattern is characteristic of an orthorhombic unit subcell usually formed by n-alkane chains[16] and should be related to β'-phase of SSS [33]. Considering the fact that two sets of lamellar peaks have been identified for mixtures containing **S_{26}**-stat-**O_{32}** and **S_{23}**-stat-**O_{67}** in SAXD (Figures 7B and 7C) where one set corresponds to a period of SSS crystallized in α-phase and the other to a shorter period, the WAXD pattern should be related to a mixture of α and β' polymorphs of SSS represented by two sets of peaks: hexagonal 100_α and orthorhombic $110_{\beta'}$ and $200_{\beta'}$, respectively.

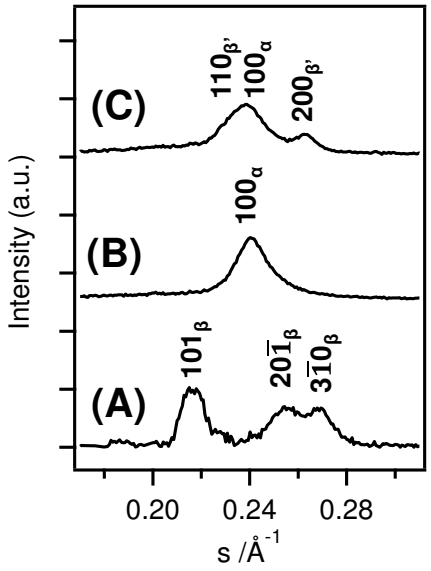

Figure 8. WAXD data obtained at 0 °C for SSS in OOO crystallized after cooling at 1 °C/min from 70 °C A) without additives and in the presence of B) **S_{37}-O_{138}**, and C) **S_{26}**-stat-**O_{32}**. OOO background scattering was subtracted from the original WAXD data. WAXD peaks of α-, β'- and β-phase of SSS are indicated by Miller indices.

The appearance of the less thermodynamically stable α-phase for SSS crystallized in the presence of **S**-containing polymeric additives implies that a strong influence is exerted by the polymer on SSS during nucleation and/or growth. Methacrylic polymers with long alkyl side chains, such as poly(stearyl methacrylate), are known to favour a mode of crystallization in which the side chains pack onto a hexagonal lattice.[35, 36] Assuming that stearyl side chains within these block copolymers behave the same way, it appears that these additives may act as epitaxial templates or directors for SSS crystallization. Similar behaviour has been observed in fat crystals dispersed by aliphatic emulsifiers in water[37]. Evidently, a continuous block of stearyl methacrylate is also a key structural feature to stabilize pure α polymorph of SSS, since statistical copolymers with smaller fractions of **S** fail to do so. This is likely due to the lower polymer crystallinity (Table 1), which is disrupted by the presence of **O** units between **S** units. Furthermore, a reduction of the stearyl chain concentration per unit length of the polymer backbone in $\mathbf{S_{23}}$-stat-$\mathbf{O_{67}}$ and $\mathbf{S_{26}}$-stat-$\mathbf{O_{32}}$ statistical copolymers allows more freedom for SSS during crystallization, enabling the rotator α-phase to transform to a thermodynamically more stable β'-phase.

Crystal microstructure analysis.

Additional information about the structure of primary TAG crystallites can be gleaned by quantitative analysis of the lamellar Bragg peak shapes and broadening. In particular, the peak breadth contains information about the size of crystallites and the presence of lattice microstrain.[21, 38, 39] SAXD data collected during in situ cooling experiments revealed that the width of the crystalline lamellar peaks varied considerably depending on the polymeric additive used. As it follows from the stacked plot of SAXD patterns (Figure 9A), there was a clear increase in the width of the 001_α peak as the fraction of **S** within the polymer decreased.

Prior literature concerning the structural analysis of fat crystals using x-ray scattering methods have employed Scherrer analysis, which relates the width of the first lamellar peak (i.e. the peak full width at half maximum, FWHM or peak integral breadth) as being inversely proportional to the crystallite thickness.[2, 11] However, this technique is limited in that it ignores higher order lamellar peaks, which provide additional information about the TAG crystal microstructure. Taking higher

order lamellar peaks into consideration enables peak broadening originating from crystallite size and crystal lattice strain to be separated. Thus, more sophisticated methods of peak broadening analysis that take strain into account such as the Williamson-Hall (WH) technique[21] could be used.

The WH analysis was applied to SAXD data obtained from the slow cooling experiments (Figure 7B). After OOO background scattering subtraction, Lorenz correction of the SAXD patterns, fitting the 001_α and 003_α diffraction peaks according to eq 5 and a further processing of the results for instrumental peak broadening using eqs 4 and 6, the physical component of the peak breadths has been calculated from eq 1 and a WH plot (β_f^* versus s) was obtained (Figure 9B). The WH plot demonstrates a significant difference between peak breadths measured for the 001_α and 003_α peaks in all samples. This immediately confirms the presence of some strain within the crystals, and highlights the limitation of Scherrer analysis in measuring the thickness of TAG crystallites.

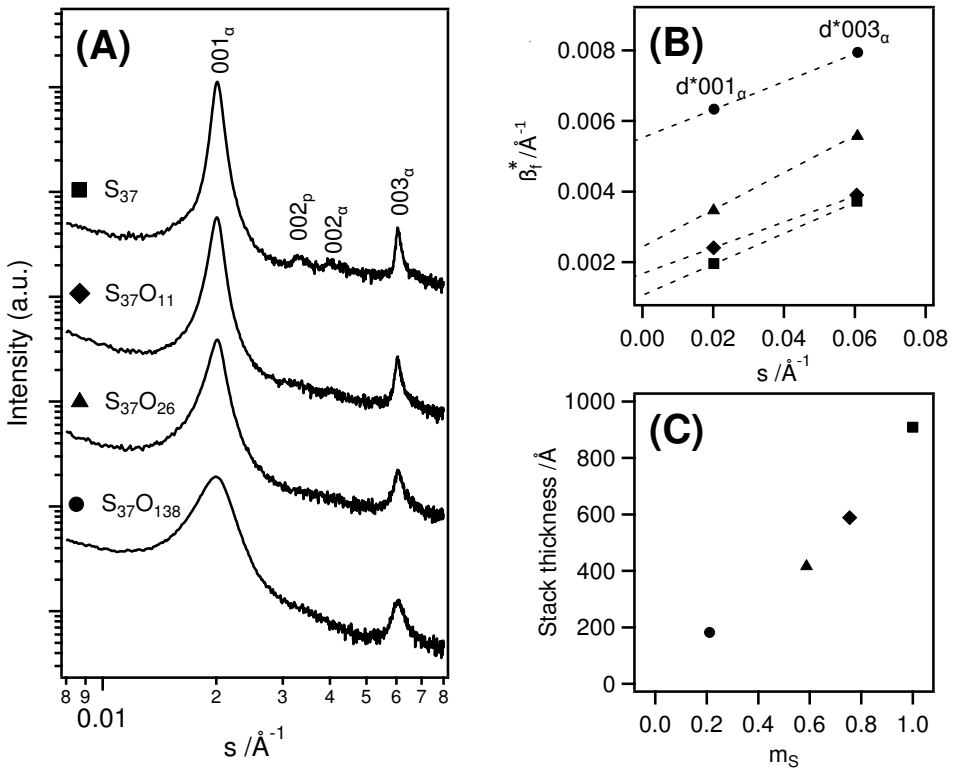

Figure 9. (A) SAXD data collected at 0 °C from SSS (5 wt% in OOO) with $\mathbf{S_{37}}$ and $\mathbf{S_{37}\text{-}O_x}$ polymer additives (indicated on the plot), after cooling at 1 °C/min from 70 °C, which were used for WH analysis. OOO background scattering was subtracted from the original SAXD data. (B) A WH plot of the peak integral breadth β_f^* versus s, obtained from analysis of the 001_α and 003_α lamellar peaks of samples prepared with different additives (accordingly labelled in A). (C) Results of WH analysis, which revealed a systematic variation in lamellar stack thickness as a function of the mass fraction of **S** within the block copolymer (m_s).

Comparison of the intercept in Figure 9B revealed that a larger fraction of **S** block within the polymer additive (m_S) led to increasing crystallite size (Figure 9C, solid symbols). Crystal lattice microstrains calculated from the gradient of the line were similar in all cases, with $e_{WH} < 0.025$, and there was no particular trend as a function of m_S (Figure S3). Thus, there is a strong evidence that differences in peak integral breadths observed in SSS crystallized in the presence of polymeric additives is mainly due to differences in TAG crystallite (likely nanoplatelet) thickness. Thinner SSS nanoplatelets (as low as 18 nm, corresponding to about four 2L SSS layers) were measured when block copolymer additives with large fractions of amorphous **O** block were employed, whilst decreasing the fraction of **O** block increased crystallite size up to a maximum of 91 nm (with $\mathbf{S_{37}}$) proportional to about twenty 2L SSS layers. The monotonic increase of crystal thickness (and the associated number of SSS layers) as a function of **S** block fraction suggests that it is possible to precisely control fat crystallite dimensions by designing the polymer additive.

Co-crystallization between polymer additives and TAGs

To better understand the interaction between polymers and SSS in the absence of OOO, DSC analyses were conducted. The solubility of polymer additives within a solvent can significantly impact on interactions with crystalline materials (e.g. waxes), and these interactions may not occur in a melt.[40] Omitting OOO from DSC measurements enabled the direct effect of polymer additives on SSS crystals to be observed, independent of solubility in OOO. Mixtures of SSS and polymers prepared with the same ratio as used in SAXD experiments (i.e. 1:2 molar ratio StMA:tristearin) were clear at 70 °C, indicating complete solubility of polymers in SSS in the liquid state. Heating and cooling cycles (10 °C/min) revealed that SSS crystallization was altered in the presence of polymer additives (Figure 10). Within the second heating cycle of SSS and all mixtures, two strong endotherm peaks were present above 40 °C, separated by an exotherm peak (Figure 10A). The first endotherm corresponds to melting of α-phase, followed by an exotherm from recrystallization into β-phase, and finally a second endotherm as the β-phase melts.[33] DSC analyses revealed that the onset temperatures of each of these melting and recrystallization events were shifted to lower temperatures in the presence of polymer additives. There was also a clear trend that as the fraction of **O** in the polymer

additive increased, the onset of SSS melting decreased. The reduction of melting point by polymeric additives is indicative of decreasing SSS crystallite size, consistent with calculations from peak broadening analysis of SAXD data, which showed that SSS crystallite size decreased as **O** fraction in the copolymer additive was increased (Figure 9C).

During the DSC cooling cycles, SSS crystallization temperature was reduced by the presence of **S**-containing polymers (Figure 10B), which also corroborates to the SAXD results in the presence of solvent (OOO). The DSC cooling cycles also revealed additional endothermic transitions at <40 °C in mixtures containing polymer additives (labelled by black diamonds in Figure 10B), apparently due to separate crystallization of polymer side chains, indicating that polymers are excluded from co-crystallizing intimately with SSS. Relative to the neat polymers, these polymer crystallization events occurred at higher temperatures in the presence of SSS, strongly suggesting that SSS crystals act as nucleating sites for polymer crystals. This observation is consistent with SAXD analyses in OOO solutions: $\mathbf{S_{37}}$ does not crystallize in OOO during the cooling cycle (Figure S4), but in the presence of SSS there is a clear evidence for the formation of $\mathbf{S_{37}}$ crystals in addition to SSS crystals (Figure S5). However, no evidence for the formation of polymer crystals formed by block or statistical copolymers was observed during SSS crystallisation from OOO solutions.

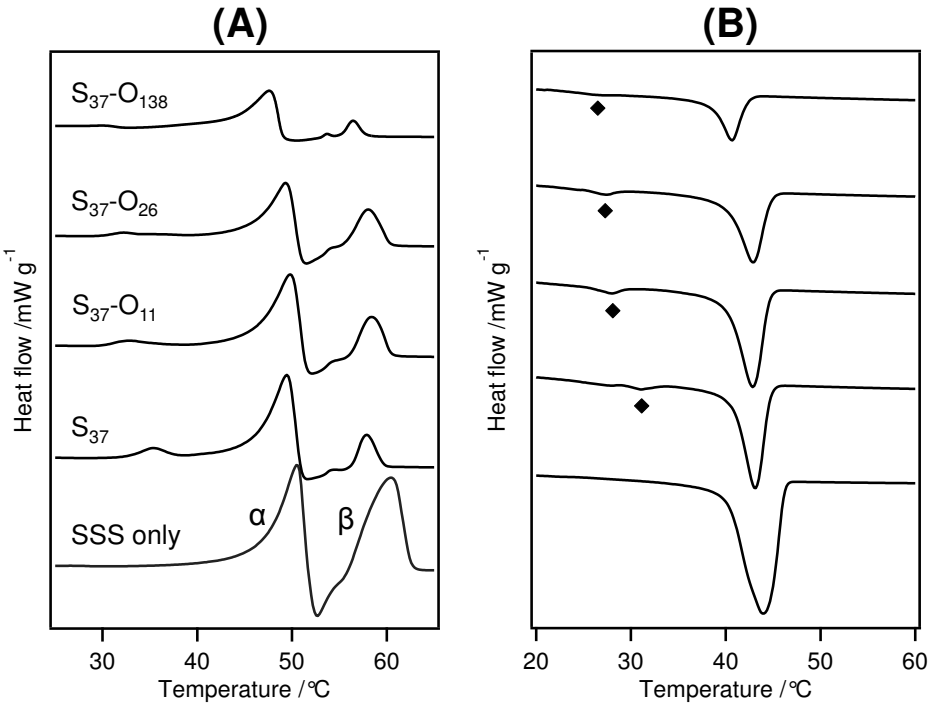

Figure 10. DSC traces recorded during the 2nd heating cycle (10 °C/min, A) and 2nd cooling cycle (10 °C/min, B) of SSS alone and in the presence of various polymeric additives (indicated on the plot). The exotherm peak resulting from crystallization of the polymeric stearyl side chains is indicated by black diamond symbols.

Data from DSC analyses support findings from SAXD analysis of solutions in OOO, and provide further insight into the interaction of polymer additives with SSS that lead to crystal habit modification.

Mechanism of Crystal Habit Modification

From the microscopy, SAXD, WAXD and DSC analyses outlined above, a possible mechanism of SSS crystal habit modification by stearyl methacrylate-containing additives can be hypothesised. In the presence of $\mathbf{S_{37}}$ and $\mathbf{S_{37}\text{-}O_x}$ block copolymer additives, the decreased crystallization temperature of SSS leads to the conclusion that van der Waals' interactions between polymeric stearyl side chains and SSS molecules in solution enhance its solubility in OOO. Upon cooling below the supersaturation temperature SSS nucleates into α-phase and polymer stearyl side chains crystallize (which would not otherwise occur under these conditions, see Figure S5). Upon further cooling, SSS molecules would ordinarily rearrange into the more thermodynamically stable β-phase, but are prevented from undergoing this polymorphic transition due to the presence of polymeric stearyl side-chains. Therefore, it is reasonable to assume that polymeric side-chains, which pack onto a hexagonal lattice, exert an epitaxial influence and pin the SSS crystals in the α-form for the duration of the cooling cycle. **S**-stat-**O** copolymers are only able to partially influence the polymorphism, and some SSS crystals transform from the α phase to the more stable β'-form. This must be the result of the amorphous segments (**O**) that interact weakly with SSS, in between semi-crystalline segments (**S**) that can pin regions of SSS crystals.

The structure of the block copolymer additive was also found to control the primary crystallite size, i.e. the average number of SSS lamellae in each nanocrystallite. In the presence of block copolymers with large fractions of **O** block, crystallites are thinner, suggesting that these polymers "poison" the TAG crystal growth normal to the lamellar layers, probably owed to the **O** block acting as a steric barrier. In the presence of $\mathbf{S_{37}}$ crystallites are almost 5 times as large, which indicates that this additive does not prevent crystal growth normal to lamellar. This may be

accentuated by the observation that the $\mathbf{S_{37}}$ additive had a higher propensity to form polymer crystals: if polymer chains crystallized separately, fewer are available to co-crystallize with SSS and influence crystal growth. Based on SAXD and DSC analyses, a larger fraction of **O** block in the copolymers decreases the amount of polymeric crystals that form independently. Overall, these results highlight an important role of the amorphous component (oleyl methacrylate) within these TAG crystal habit modifiers: to act as a steric barrier that limits the growth of TAG crystals, and to prevent the formation of large polymer crystals.

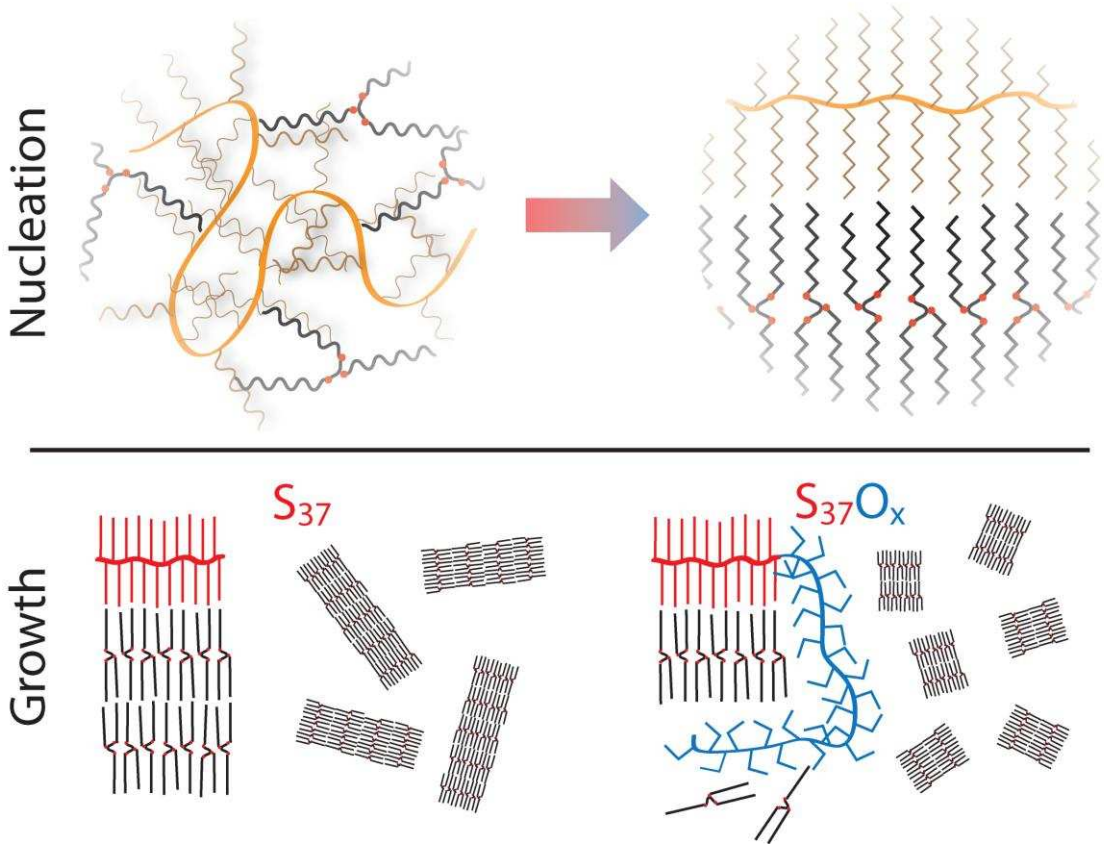

Figure 11: Schematic representation of the proposed mechanism poly(stearyl methacrylate) and poly(stearyl methacrylate)-containing block copolymers exert control over SSS crystallization.

As demonstrated from microscopy analysis, addition of polymers during SSS crystallization strongly influences the macroscopic appearance of SSS crystals. Given the highly hierarchical nature of TAG crystallization and the nanoscale size of primary crystallites, the different appearance of SSS crystals at the micrometer length-scale alludes to an effect of polymeric additives on the crystallite aggregation. In particular, the dendritic structures that are characteristic of unadulterated TAG

crystallization (i.e. Figure 3A), do not form in the presence of polymeric additives. Instead, smaller crystals with more regular shapes result when **S**-containing polymers are present. The observation that block copolymers containing large fractions of **O** produce highly uniform spherulitic crystals suggests that the large amorphous block plays an important role in aggregation of SSS crystals.

Conclusions

This paper has outlined the impact of polymer additives containing poly(stearyl methacrylate) on the crystallization of the ubiquitous triacylglycerol fat, tristearin (SSS). A library of bottlebrush-like block and statistical copolymers with amorphous poly(oleyl methacrylate) component were synthesized by RAFT-controlled polymerization. Addition of these polymers to solutions of SSS in OOO resulted in more uniform SSS crystals with diverse and controllable morphologies, upon cooling. In situ SAXD/WAXD analyses during cooling of SSS solutions in OOO demonstrated that the presence of poly(stearyl methacrylate) and **S**-containing block polymers affected the SSS crystallization temperature, the thickness of primary crystallites and the final polymorph, and thus acted as fat crystal habit modifiers.

Results obtained with this library of polymers outline some important design rules when designing additives to control fat crystallization at different length-scales. (1) In the absence of additives, SSS in OOO tends to nucleate as α-phase before rearranging into the more thermodynamically stable β-polymorph. In order to prevent this polymorphic transition and favour α-phase, it is necessary to have a continuous sequence of stearyl methacrylate monomers (i.e. a block). A statistical distribution of stearyl and oleyl methacrylate monomers led to some rearrangement into β'-phase. (2) By changing the fraction of crystalline monomer within the additive, the thickness of SSS crystallites can be controlled. There is a clear trend amongst block copolymers that increasing the content of amorphous monomer reduces the crystallite thickness, which could be finely tuned in the present study from 20 to 90 nm (that is, from 4 to 20 TAG layers) by selecting the ratio of the two monomers. (3) Changing the fraction of crystalline monomer within the additive enables control of the overall crystal morphology . When stearyl-rich additives are used, the crystals tend to aggregate into needle-like particles. Increasing the content of amorphous oleyl units lead to uniform 3-

dimensional spherulitic structures. These results demonstrate a profound effect of the semi-crystalline monomer content on the aggregation of primary crystallites.

Exploiting these additives to simultaneously manipulate the packing of TAG molecules within lamellae, the size of primary crystallites, and the macroscopic crystal morphology could diversify the range of fat material properties and supplement applications in areas ranging from personal care to small molecule delivery.[12]

Supporting Information

The Supporting Information is available free of charge on the ACS Publications website at DOI:

Representative WAXD patterns for crystallization of SSS (5 wt% in OOO) in the presence of stearyl methacrylate-based polymers (**O_{67}**, **S_{37}**, **$S_{37}O_{11}$**, **S_{37} O_{26}**), crystal strain lattice values measured by WH analysis, time-resolved SAXD for isothermal treatment of **S_{37}** in OOO (1wt %) at 30 °C, and SAXD patterns of pure **S_{37}** after crystallization.

Acknowledgements

O.O.M. thanks EPSRC for the capital equipment grant to purchase the laboratory-based Xenocs/Excillum SAXS instrument used for characterizing the studied TAG mixtures (EP/M028437/1). A.J.R and O.O.M thank Unilever R & D for PDRA funding for J.J. Special thanks to Dave Thornthwaite at Unilever R & D for fruitful discussions.

References

1. Marangoni, A. G.; Acevedo, N.; Maleky, F.; Co, E.; Peyronel, F.; Mazzanti, G.; Quinn, B.; Pink, D. Structure and functionality of edible fats. *Soft Matter* **2012,** *8*, 1275-1300.
2. Acevedo, N. C.; Marangoni, A. G. Toward nanoscale engineering of triacylglycerol crystal networks. *Cryst. Growth Des.* **2010,** *10*, 3334-3339.
3. Acevedo, N. C.; Marangoni, A. G. Nanostructured Fat Crystal Systems. *Annu. Rev. Food Sci. Technol.* **2014,** *6*, 1-26.
4. Peyronel, F.; Quinn, B.; Marangoni, A. G.; Pink, D. a. Ultra small angle x-ray scattering in complex mixtures of triacylglycerols. *J. Phys. Condens. Matter* **2014,** *26*, 464110-464110.
5. Oh, J. H.; McCurdy, A. R.; Clark, S.; Swanson, B. G. Stabilizing polymorphic transitions of tristearin using diacylglycerols and sucrose polyesters. *J. Am. Oil Chem.' Soc.* **2005,** *82*, 13-19.

6. Miskandar, M. S.; Che Man, Y. B.; Abdul Rahman, R.; Nor Aini, I.; Yusoff, M. S. A. Effects of emulsifiers on crystal behavior of palm oil blends on slow crystallization. *J. Food Lipids* **2007,** *14*, 1-18.
7. Shimamura, K.; Ueno, S.; Miyamoto, Y.; Sato, K. Effects of Polyglycerine Fatty Acid Esters Having Different Fatty Acid Moieties on Crystallization of Palm Stearin. *Cryst. Growth Des.*, **2013**, *13*, 4746–4754
8. Verstringe, S.; Dewettinck, K.; Ueno, S.; Sato, K. Triacylglycerol crystal growth: Templating effects of partial glycerols studied with synchrotron radiation microbeam x-ray diffraction. *Cryst. Growth Des.* **2014,** *14*, 5219-5226.
9. Tran, T.; Green, N. L.; Rousseau, D. Spheroidal Fat Crystals: Structure Modification via Use of Emulsifiers. *Cryst. Growth Des.* **2015,** *15*, 5406-5415.
10. El Kinawy, O. S.; Petersen, S.; Bergt, K.; Ulrich, J. Influence of emulsifiers on the formation and crystallization of solid lipid nanoparticles. *Chem. Eng. Technol.* **2013,** *36*, 2174-2178.
11. Acevedo, N. C.; Marangoni, A. G. Characterization of the Nanoscale in Triacylglycerol Crystal Networks. *Cryst. Growth Des.* **2010,** *10*, 3327-3333.
12. Gunstone, F. D.; Padley, F. B. *Lipid Technologies and Applications*. Marcel Dekker: New York, 1997; p 834.
13. Hosta-Rigau, L.; Chandrawati, R.; Saveriades, E.; Odermatt, P. D.; Postma, A.; Ercole, F.; Breheney, K.; Wark, K. L.; Städler, B.; Caruso, F. Noncovalent Liposome Linkage and Miniaturization of Capsosomes for Drug Delivery. *Biomacromolecules* **2010,** *11*, 3548-3555.
14. Sato, K.; Ueno, S. Molecular Interactions and Phase Behavior of Polymorphic Fats. In *Crystallization Processes in Fats and Lipid Systems*, Sato, K.; Garti, N. Eds. Marcel Dekker: New York, 2001; pp 177-209.
15. Mykhaylyk, O. O.; Hamley, I. W. The Packing of Triacylglycerols from SAXS Measurements: Application to the Structure of 1,3-Distearoyl-2-oleoyl- sn -glycerol Crystal Phases. *J. Phys. Chem. B* **2004,** *108*, 8069-8083.
16. Small, D. M. *The Physical Chemistry of Lipids*. Plenum Press: New York, 1986; p 672.
17. Enzo, S.; Fagherazzi, G.; Benedetti, A.; Polizzi, S. A Profile-fitting Procedure for Analysis of Broadened X-ray-Diffraction Peaks .1. Methodology. *J. App. Cryst.* **1988,** *21*, 536-542.
18. Langford, J. I.; Delhez, R.; Dekeijser, T. H.; Mittemeijer, E. J. Profile Analysis for Microcrystalline Properties by the Fourier and other methods. *Aust. J. Phys.* **1988,** *41*, 173-187.
19. Warren, B. E.; Averbach, B. L. The effect of cold-work distortion on x-ray patterns. *J. Appl. Phys.* **1950,** *21*, 595-599.
20. Warren, B. E.; Averbach, B. L. The separation of cold-work distortion and particle size broadening in x-ray patterns. *J. Appl. Phys.* **1952,** *23*, 497-497.
21. Williamson, G. K.; Hall, W. H. X-ray line broadening from filed aluminium and wolfram. *Acta Metallurgica* **1953,** *1*, 22-31.
22. Dekeijser, T. H.; Langford, J. I.; Mittemeijer, E. J.; Vogels, A. B. P. Use of the voigt function in a single-line method for the analysis of x-ray-diffraction line broadening. *J. Appl. Cryst.* **1982,** *15*, 308-314.
23. Langford, J. I. Rapid method for analyzing breadths of diffraction and spectral-lines using voigt function. *J. Appl. Cryst.* **1978,** *11*, 10-14.
24. Wilson, A. J. C. *Mathematical theory of X-ray powder diffractometry*. Philips Technical Library: Eindhoven, 1963; p 128.
25. Young, R. A.; Wiles, D. B. Profile shape functions in rietveld refinements. *J. Appl. Cryst.* **1982,** *15*, 430-438.
26. Halder, N. C.; Wagner, C. N. J. Separation of particle size and lattice strain in integral breadth measurements. *Acta Crystallographica* **1966,** *20*, 312-313.
27. vanBerkum, J. G. M.; Delhez, R.; deKeijser, T. H.; Mittemeijer, E. J. Diffraction-line broadening due to strain fields in materials; Fundamental aspects and methods of analysis. *Acta Crystallographica A* **1996,** *52*, 730-747.

28. Delhez, R.; Dekeijser, T. H.; Mittemeijer, E. J. Determination of crystallite size and lattice-distortions through x-ray-diffraction line-profile analysis - recipes, methods and comments. *Fresenius Zeitschrift Fur Analytische Chemie* **1982,** *312*, 1-16.
29. Roisnel, T.; Rodriguez-Carvajal, J. WinPLOTR: A Windows tool for powder diffraction pattern analysis. In *Epdic 7: European Powder Diffraction, Pts 1 and 2*, 2001; Vol. 378-3, pp 118-123.
30. Chiefari, J.; Chong, Y. K.; Ercole, F.; Krstina, J.; Jeffery, J.; Le, T. P. T.; Mayadunne, R. T. A.; Meijs, G. F.; Moad, C. L.; Moad, G.; Rizzardo, E.; Thang, S. H. Living Free-Radical Polymerization by Reversible Addition-Fragmentation Chain Transfer: The RAFT Process. *Macromolecules* **1998,** *31*, 5559-5562.
31. Moad, G.; Rizzardo, E.; Thang, S. H. Living radical polymerization by the RAFT process. *Aust. J. Chem.* **2005,** *58*, 379-410.
32. Mykhaylyk, O. O.; Martin, C. M. Effect of unsaturated acyl chains on structural transformations in triacylglycerols. *Eur. J.Lipid Sci. Technol.* **2009,** *111*, 227-235.
33. Lavigne, F.; Bourgaux, C.; Ollivon, M. Phase transitions of saturated triglycerides. *J. Phys. IV France* **1993,** *3*, C8-137-C8-140.
34. van Langevelde, A.; van Malssen, K.; Hollander, F.; Peschar, R.; Schenk, H. Structure of mono-acid even-numbered [beta]-triacylglycerols. *Acta Crystallographica B* **1999,** *55*, 114-122.
35. Hempel, E.; Budde, H.; Höring, S.; Beiner, M. On the crystallization behavior of frustrated alkyl groups in poly(n-octadecyl methacrylate). *J. Non-Cryst. Solids* **2006,** *352*, 5013-5020.
36. Inomata, K.; Sakamaki, Y.; Nose, T.; Sasaki, S. Solid-State Structure of Comb-Like Polymers Having n-Octadecyl Side Chains I. Cocrystallization of Side Chain with n-Octadecanoic Acid. *Polym. J.* **1996,** *28*, 986.
37. Ishibashi, C.; Hondoh, H.; Ueno, S. Epitaxial Growth of Fat Crystals on Emulsifier Crystals with Different Fatty Acid Moieties. *Cryst. Growth Des.* **2017,** *17*, 6363-6371.
38. Mykhaylyk, O. O.; Gadzira, M. P. Arrangement of C atoms in the SiC–C solid solution. *Acta Crystallographica B* **2007,** *55*, 297-305.
39. Enzo, S.; Fagherazzi, G.; Benedetti, A.; Polizzi, S. A profile-fitting procedure for analysis of broadened X-ray diffraction peaks. I. Methodology. *J. Appl. Cryst.* **2007,** *21*, 536-542.
40. Binks, B. P.; Fletcher, P. D. I.; Roberts, N. A.; Dunkerley, J.; Greenfield, H.; Mastrangelo, A.; Trickett, K. How polymer additives reduce the pour point of hydrocarbon solvents containing wax crystals. *Phys. Chem. Chem. Phys.* **2015,** *17*, 4107-4117.